JOURNAL OF CATALYSIS **177,** 343–351 (1998)
ARTICLE NO. CA982143

Structure and Properties of Vanadium Oxide–Zirconia Catalysts for Propane Oxidative Dehydrogenation

Andrei Khodakov, Jun Yang, Stephen Su, Enrique Iglesia,[1] and Alexis T. Bell[1]

Chemical Sciences Division, Lawrence Berkeley National Laboratory, and Department of Chemical Engineering, University of California, Berkeley, California 94720-1462

Received December 22, 1997; revised April 8, 1998; accepted April 28, 1998

The structure of vanadia species supported on zirconia depends on VO_x surface density and on the temperature of catalyst oxidation pretreatments. X-ray diffraction and Raman and UV-visible spectroscopies show that supported VO_x species form polyvanadate domains of increasing size and ultimately monolayers and clusters as vanadium surface density increases. Initial propene selectivities in oxidative dehydrogenation of propane at 606 K increase with increasing VO_x surface density and reach constant values of 80% at surface densities of about 2–3 VO_x/nm^2. High selectivities to CO_x products at low surface densities and on bulk ZrV_2O_7 appear to be associated with exposed unselective V–O–Zr and Zr–O–Zr sites. Propane oxidative dehydrogenation rates increase initially as the size of polyvanadate domains increases with increasing VO_x surface density. Oxidative dehydrogenation rates decreases eventually as the formation of V_2O_5 clusters at high surface densities leads to a decrease in the fraction of VO_x exposed at cluster surfaces. The ratio of rate constants for propane oxidative dehydrogenation and propene combustion to CO_x remains constant throughout the entire range of VO_x surface density (0.4–100 VO_x/nm^2), suggesting that primary oxidative dehydrogenation steps and secondary oxidation reactions of desired propene products require identical polyvanadate structures.

INTRODUCTION

Selective dehydrogenation of alkanes remains a formidable challenge for the wider use of alkanes as feedstocks. Thermal dehydrogenation of light alkanes to olefins is thermodynamically favorable at high temperatures, but often leads to high yields of coke and smaller hydrocarbons. Oxidative dehydrogenation (ODH) of alkanes is thermodynamically favored at much lower temperatures, but it requires a selective catalyst in order to avoid complete oxidation to CO and CO_2. A number of recent studies have shown that catalysts based on supported vanadium oxide show promise for ODH of C_2–C_4 alkanes (1–17). The activity and selectivity of such catalysts depends on the composition of the support, the manner in which vanadia is dispersed and in which the catalyst is pretreated (1, 3, 4, 18, 19). Basic metal oxide supports, such as MgO, Bi_2O_3, La_2O_3, Sm_2O_3, produce catalysts with higher alkene selectivity than acidic oxides, such as SiO_2, TiO_2, Al_2O_3 (7, 8), but other factors, such as the structure of the vanadia overlayer may be important (18, 19). Efforts aimed at relating the structure of the dispersed vanadia to its catalyst activity and selectivity suggest that both isolated tetrahedral V^{5+} species and oligomeric tetrahedral V^{5+} species can provide active and selective sites for alkane ODH; however, the catalytic performance of supported vanadia catalysts also depends on the distance between the selective sites (1, 3, 4, 10–12, 18–20).

Few previous studies of alkane ODH reactions have focused on VO_x species supported on ZrO_2 (21–23). Yet, ZrO_2 is an excellent support for the synthesis of highly dispersed oxides. Zirconia can be prepared with high surface area (>300 m^2/g) and it can be maintained at relatively high values even after oxidation at high temperatures (24, 25). Also, in contrast with more weakly interacting supports, such as SiO_2, ZrO_2 inhibits the sintering of supported oxides (e.g., WO_3 (26), MoO_3 (27)) in the presence of water at high temperatures. Finally, zirconia is chemically stable, inactive in oxidative reactions, and does not reduce at conditions of alkane ODH reactions.

The objective of our study was to determine the relationship between the structure of vanadia dispersed on zirconia and their catalytic activity and selectivity in propane ODH. The structures of the zirconia support and of the dispersed vanadia were characterized by several techniques. The surface areas of the catalysts were determined by the BET method. X-ray diffraction (XRD), Raman spectroscopy, and UV-Visible spectroscopy were used to characterize the structure and electronic properties of the support and the dispersed vanadia. The catalytic behavior of these solids in the ODH of propane was determined using a flow reactor equipped with on-line gas chromatographic analysis. An important element of the work was to establish the influence of vanadium surface density, and of the

[1] Authors to whom correspondence should be addressed.

0021-9517/98 $25.00

temperature of oxidative pretreatments on catalyst activity and selectivity.

EXPERIMENTAL

Zirconium oxyhydroxide ($ZrO(OH)_2$) was prepared by precipitation from a zirconyl chloride solution (98%, Aldrich, Inc.) at a pH of 10, held constant by controlling the rate of addition of a solution of ammonium hydroxide (29.8%, Fischer Sci., Inc.). After precipitation, the solids were washed with mildly basic ammonia hydroxide solution (pH ~8) until the effluent showed no chloride ions by a silver nitrate test. The resulting solids were dried in air overnight at 393 K.

VO_x/ZrO_2 catalysts (Table 1) were prepared by incipient wetness impregnation of the precipitated zirconium oxyhydroxide with a solution of ammonium metavanadate (99%, Aldrich, Inc.) (28). This solution was prepared by mixing ammonium metavanadate with oxalic acid (Mallinckrodt, analytical grade). The mixture (NH_4VO_3/oxalic acid = 1/2 molar) was heated and stirred until clear before impregnating the support. Vanadium concentrations in solution were varied in order to ensure the desired VO_x concentrations in the catalyst. After impregnation, samples were dried overnight in air at 393 K and treated in dry air at 673, 773, or 873 K for 3 h.

Bulk V_2O_5 was prepared by decomposing ammonium metavanadate in air at 773 K for 3 h. Zirconium vanadate ZrV_2O_7 (21) was prepared by heating a stoichiometric mixture of V_2O_5 and ZrO_2 in air at 923 K for 120 h, during which the sample was removed from the furnace and ground three times. The sample temperature was then raised to 983 K for 48 h, during which time the sample was removed once for grinding.

TABLE 1

Synthesis Procedure and Surface Areas of VO_x/ZrO_2 Samples

Sample	Preparation procedure	Wt% V_2O_5	S_{BET} after drying at 393 K (m^2/g)
ZrO_2	$ZrOCl_2$, precipitation at pH = 10	0	330
$2VO_x/ZrO_2$	Impregnation of $ZrO(OH)_2$ with NH_4VO_3	2	340
$5VO_x/ZrO_2$	Impregnation of $ZrO(OH)_2$ with NH_4VO_3	5	285
$10VO_x/ZrO_2$	Impregnation of $ZrO(OH)_2$ with NH_4VO_3	10	220
$15VO_x/ZrO_2$	Impregnation of $ZrO(OH)_2$ with NH_4VO_3	15	180
$30VO_x/ZrO_2$	Impregnation of $ZrO(OH)_2$ with NH_4VO_3	30	180
ZrV_2O_7	Solid state reaction of V_2O_5 and ZrO_2	60	<1
V_2O_5	Thermal decomposition of NH_4VO_3 (773 K)	100	3

Surface areas were measured in a N_2 physisorption apparatus equipped with a thermal conductivity detector using the single-point BET method. Before measurements, samples pretreated above 673 K were dehydrated in He at 473 K for 1 h; the samples dried at 393 K were dehydrated in He at 393 K for 2 h in order to prevent structural changes at higher air pretreatment temperatures.

Powder XRD measurements were carried out at room temperature using Cu (K_α) radiation and a Siemens diffractometer. A small amount of catalyst was mixed with vaseline and spread out smoothly on a thin glass plate placed into the diffractometer.

Raman spectra were recorded using the apparatus described in reference (29). Samples (0.1 g) were pressed at 70 MPa pressure into 13-mm diameter wafers of 1-mm thickness. This wafer was mounted in a quartz cell. The cell can be heated to 873 K and gases can be introduced for *in situ* measurements of catalyst samples. Raman spectra were recorded in the 250 to 1300 cm^{-1} range using the 514.5 nm argon ion laser line.

Diffuse reflectance UV-Vis spectra were recorded on a Varian-Cary 4 spectrophotometer equipped with a Harrick diffuse-reflectance attachment. MgO was used as a reference. Reflectance measurements were converted to absorption spectra using the Kubelka–Munk function (30). The sample cell was equipped with a heater unit, a water cooling system, a thermocouple and a gas circulation system. UV-Vis spectra were measured in the range of 1.5–6.0 eV at room temperature under ambient conditions.

Selectivity and rate measurements were carried out in a fixed-bed quartz reactor using 0.015–0.3 g of catalyst. Quartz powder (0.5 g) was added in order to prevent temperature gradients. The feed consisted of propane and oxygen at 14.03 and 1.74 kPa, respectively with He as a diluent. On-line analysis of reactants and products was performed using a Hewlett-Packard 5880 gas chromatograph equipped with a Carboxen column. Only C_3H_6, H_2O, CO, and CO_2 were detected as reaction products.

C_3H_8 and O_2 conversions were varied by changing the feed flow rate between 30 and 340 cm^3/min. Typical propane conversions were less than 1% and oxygen conversions were below 20%. Reaction rates and selectivities were extrapolated to zero oxygen conversion in order to determine the relative rates of primary dehydrogenation and oxidation reactions. Oxidative dehydrogenation rates and selectivities were also measured on two bulk vanadium compounds: V_2O_5 and ZrV_2O_7. Larger amounts of V_2O_5 and ZrV_2O_7 amounts were loaded into reactor in order to achieve conversion levels similar to those obtained on VO_x/ZrO_2 catalysts. Blank experiments using pure ZrO_2 or an empty reactor showed that reaction rates were negligible in the absence of VO_x species.

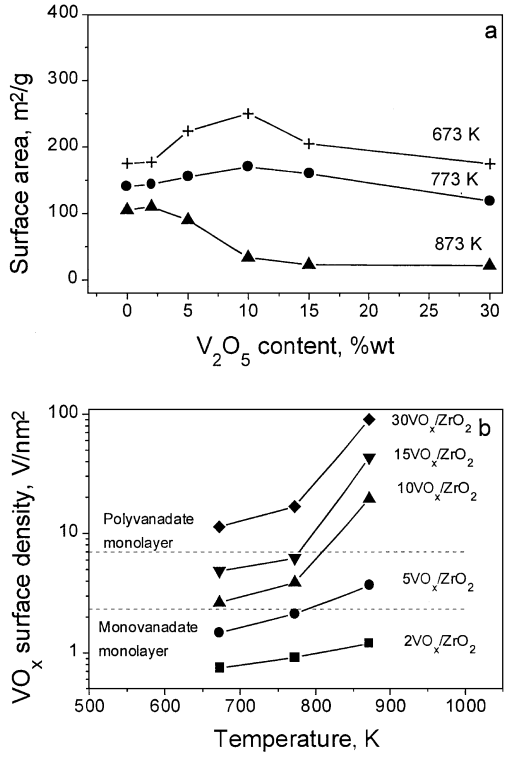

FIG. 1. Surface areas (a) and apparent VO_x surface densities (b) of VO_x/ZrO_2 catalysts calcined at different temperatures.

RESULTS

Catalyst Characterization

Catalyst surface areas and VO_x surface densities after calcination at various temperatures are shown in Figs. 1a and b. For both pure ZrO_2 and VO_x/ZrO_2 the surfaces areas decrease with increasing calcination temperature. VO_x species inhibited sintering during oxidation at 673 and 773 K for V_2O_5 loadings below 10 wt% , but the opposite effect was observed at higher loadings. When calcination is carried out at 873 K, vanadia addition causes a progressive decrease in surface area with increasing loading.

The effects of vanadia loading and calcination temperature on the apparent surface density of VO_x species are presented in Fig. 1b. Horizontal lines are shown for the VO_x densities at monolayer coverages, assuming that the monolayers consist of either monovanadate or polyvanadate species; vanadium surface densities are 2.3 VO_x/nm^2 for a monovanadate monolayer and 7.5 VO_x/nm^2 for a polyvanadate monolayer (18). At each vanadia concentration, the VO_x surface density increases with calcination temperature, because of a decrease in the ZrO_2 surface area. XRD patterns of samples calcined at 673 K are shown in Fig. 2a. After calcination at 673 K, samples with high vanadium contents (>5 wt% as V_2O_5) show no diffraction peaks. Tetragonal ZrO_2 phases are detected in samples with lower V_2O_5 loadings. Oxidation temperatures above 673 K lead to ZrO_2 crystallization. XRD patterns of samples calcined at 773 and 873 K are shown in Figs. 2b and 2c. After oxidation at 773 K, tetragonal and monoclinic phases of zirconia were detected. The relative abundance of the two phases in samples treated at 773 K depends on the vanadium content. At higher V_2O_5 contents (>5 wt% as V_2O_5), tetragonal ZrO_2 is the predominant structure. The relative amounts of tetragonal and monoclinic ZrO_2 for samples treated at 773 K were calculated using an empirical correlation proposed in (31) and shown for samples treated at 773 K

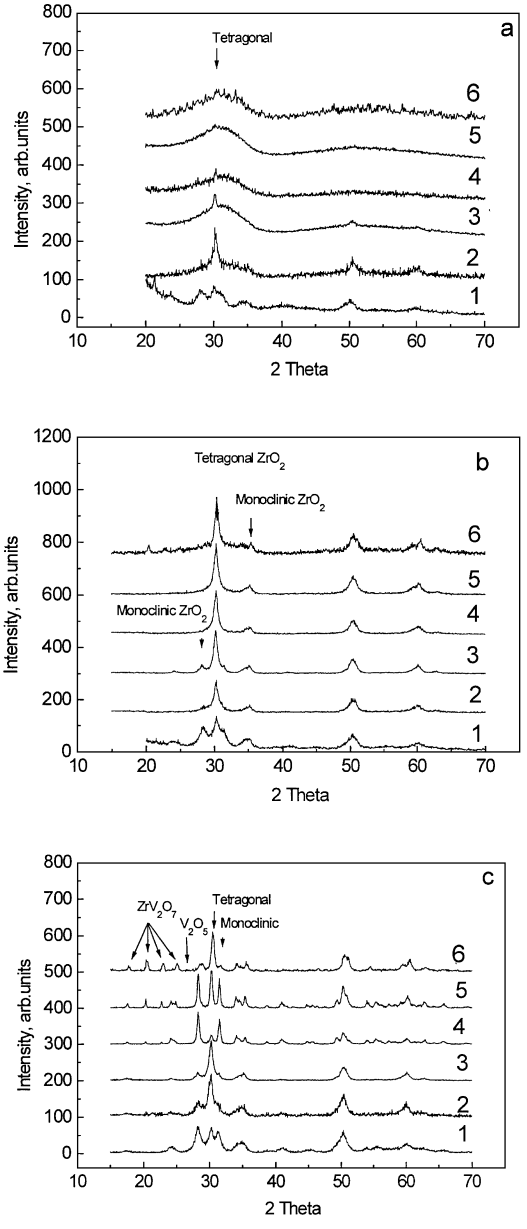

FIG. 2. XRD patterns of VO_x/ZrO_2 catalysts calcined at 673 K (a), 773 K (b), 873 K (c) (1, ZrO_2; 2, $2VO_x/ZrO_2$; 3, $5VO_x/ZrO_2$; 4, $10VO_x/ZrO_2$; 5, $15VO_x/ZrO_2$; 6, $30VO_x/ZrO_2$).

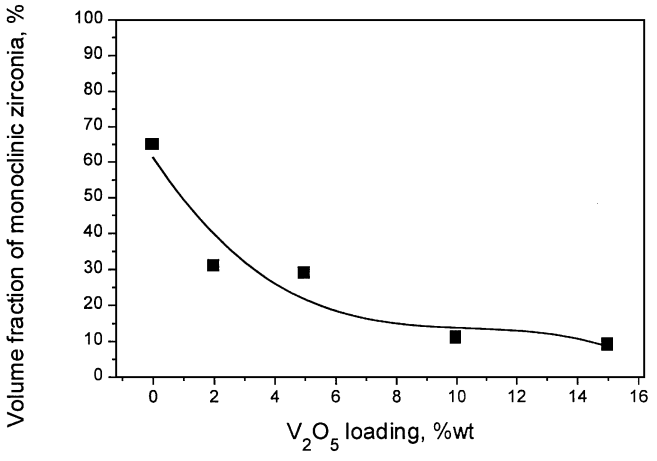

FIG. 3. Volume fraction of monoclinic ZrO_2 in VO_x/ZrO_2 catalysts calcined at 773 K.

in Fig. 3. Calcination at 873 K leads to higher conversions of ZrO_2 to the monoclinic phase and to the appearance of zirconium vanadate (ZrV_2O_7). The concentration of zirconium vanadate increases with increasing vanadium content. V_2O_5 structures are detected by XRD in samples with vanadia contents above 10 wt% and calcined at 873 K.

Raman spectra of $2VO_x/ZrO_2$ and $10VO_x/ZrO_2$ are shown in Figs. 4a and 4b, respectively. After calcination at 673 K, the only features seen in the spectrum of $2VO_x/ZrO_2$ are weak bands for monoclinic ZrO_2 located at 380, 490, and 640 cm^{-1} (32). Calcination of this sample at 873 K led to the appearance of a broad feature centered at 860 cm^{-1} and a peak at 1025 cm^{-1}. The bands associated with ZrO_2 disappeared. The band at 860 cm^{-1} was observed previously in samples of VO_x/Al_2O_3 (33, 34) and was assigned to V−O−V vibrations in polyvanadate structures. The band at 1025 cm^{-1} is attributed to V=O vibrations.

For $10VO_x/ZrO_2$, the 860 cm^{-1} feature appears after treatment at much lower temperature (673 K) than for the $2VO_x/ZrO_2$ sample (873 K). Calcination of the $10VO_x/ZrO_2$ sample at 773 K increases the intensity of this band; however, raising the calcination temperature to 873 K causes the disappearance of the band at 860 cm^{-1}, and the appearance, instead of a sharp band at 780 cm^{-1}, together with weaker features, at 500, 530, 640, and 990 cm^{-1}, due to bulk V_2O_5. The band at 780 cm^{-1} has been observed previously in the spectra of ZrV_2O_7 (21), and the remaining bands are characteristic of bulk V_2O_5.

Diffuse reflectance UV-Vis spectra of VO_x/ZrO_2 samples pretreated at 673 K are shown in Fig. 5. The bands observed in the range of 2–4 eV arise from low-energy O^{2-} to V^{5+} charge-transfer (35–38). For V^{4+} species, such transitions occur at higher energies (4.5–5 eV). The energy of an electronic transition can be characterized by the position of the energy of maximum absorption, but charge transfer bands are usually broad. Therefore, it is more useful to

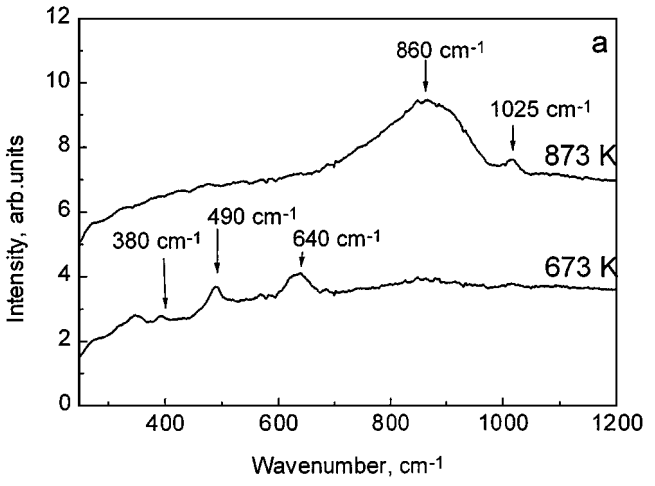

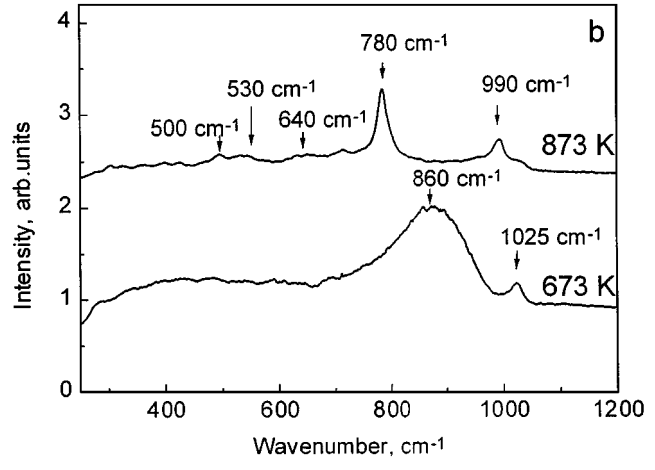

FIG. 4. Raman spectra of $2VO_x/ZrO_2$ (a) and $10VO_x/ZrO_2$ (b) samples calcined at 673 and 873 K.

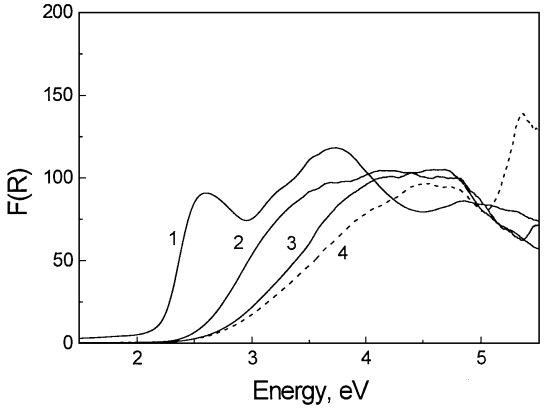

FIG. 5. Diffuse reflectance UV-Vis spectra of VO_x/ZrO_2 catalysts calcined at 673 K (1, V_2O_5; 2, $30VO_x/ZrO_2$; 3, $15VO_x/ZrO_2$; 4, $2VO_x/ZrO_2$) and then exposed to ambient conditions.

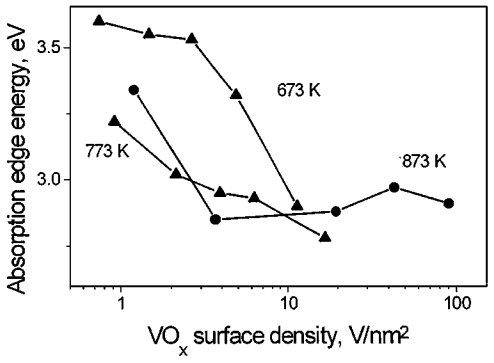

FIG. 6. Dependence of the UV-Vis absorption edge energy on the VO_x surface density and calcination temperature. All spectra were recorded under ambient conditions.

characterize the charge-transfer transition by the energy at the absorption edge, which we define as the first inflection point in the Kubelka–Munk function.

Absorption edge energies for the VO_x/ZrO_2 samples are shown in Fig. 6. For samples calcined at 673 and 773 K, the absorption edge energy decreases monotonically with increasing VO_x surface density. At a given surface density, the edge energy is lower after calcination at 773 K than after calcination at 673 K. When calcination is carried out at 873 K, the absorption edge energy first decreases with increasing VO_x surface density and then reaches a broad minimum.

Recent studies have shown that the energy of charge transfer transition can detect changes in domain size in semiconductors and solids. Higher energy of charge transfer transition are observed as the domain size of semiconductors decreases (39–46). The observed changes in the absorption edge energy as VO_x density increases are consistent with an increase in the size of the vanadia domains. Table 2 shows that as the number of vanadia polyhedrons in the first coordination shell of a V atom increases, the absorption edge energy decreases monotonically. It is also noted that the adsorption energy edge for VO_x species lies in the range of 2–4, eV, well removed from the absorption energy edge of ZrO_2 (4.99 eV) (48).

TABLE 2

UV-Vis Absorption Edge Energies in Reference Compounds

	Absorption edge energy (eV)	Number of vanadium polyhedrons in the first coordination shell
V_2O_5	2.36	5
$(NH_4)_3H_3V_{10}O_{28}$	2.50	4.8
NH_4VO_3	3.38	2
$OV[OSi(OtBu)_3]_4$	4.6	0
$VO^{2-}_{4\,(aq)}$	4.33 (47)	0
ZrO_2	4.99 (48)	—

Note. The number of next vanadium neighbors is defined as the average number of vanadium atoms located at the distances smaller than 4 Å from a V atom.

Figures 7 and 8 show C_3H_6, CO, and CO_2 selectivities and O_2 conversion as functions of residence time on $2VO_x/ZrO_2$ and $10VO_x/ZrO_2$ calcined at 673 and 873 K. Selectivity to propene is higher when $2VO_x/ZrO_2$ is calcined at 873 K instead of 673 K. At higher vanadium contents, however, propene selectivity is less sensitive to calcination temperature (Fig. 8). The selectivity to propene increases and the selectivities to CO and CO_2 decrease as contact time decreases, extrapolation to zero residence time gives the selectivity of primary reactions.

The selectivities to C_3H_6 and CO_x and the propane conversion rates at zero residence time are shown in Figs. 9 and 10, respectively, as functions of VO_x surface density.

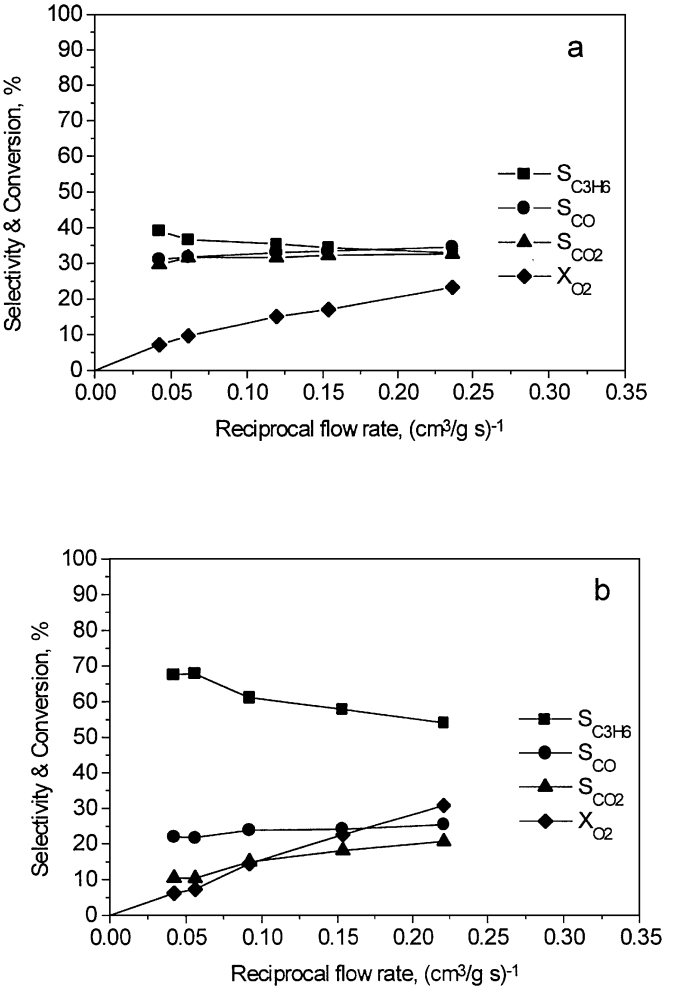

FIG. 7. Product selectivities and oxygen conversion for propane ODH over $2VO_x/ZrO_2$ catalysts treated at (a) 673 and (b) 873 K. Reaction conditions: $T = 606$ K; $P_{C_3H_8} = 14.03$; kPa; $P_{O_2} = 1.74$ kPa; weight of catalyst = 0.225 g.

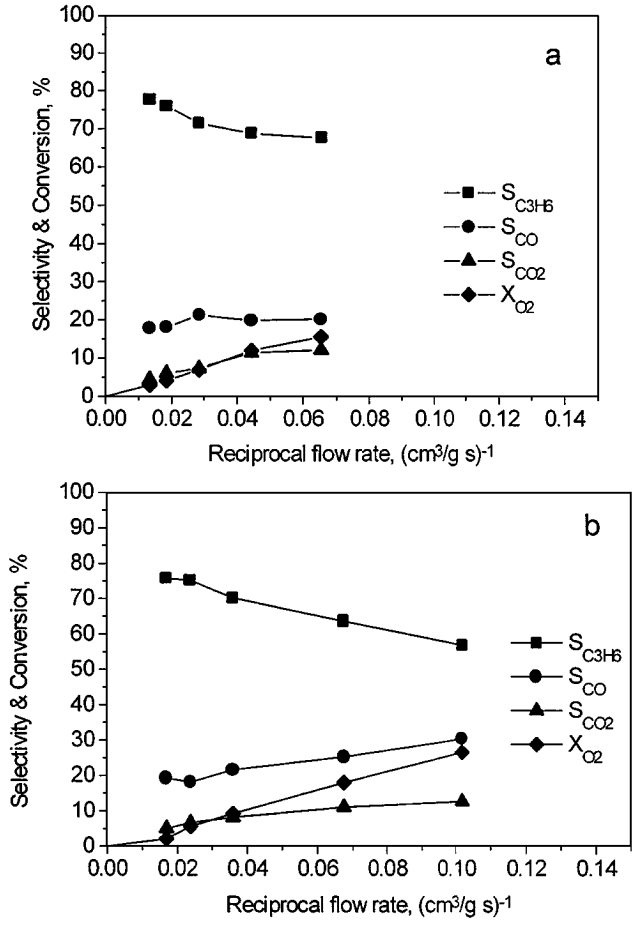

FIG. 8. Product selectivities and oxygen conversion for propane ODH over $10VO_x/ZrO_2$ catalysts treated at (a) 673 and (b) 873 K. Reaction conditions: $T = 606$ K, $P_{C_3H_8} = 14.03$ kPa, $P_{O_2} = 1.74$ kPa, weight of catalyst = 0.045 g.

Figure 9 shows that for VO_x densities below 2–3 V/nm^2 the selectivity to C_3H_6 increases with increasing surface density. Above 3 V/nm^2, the selectivity to C_3H_6 is about 80%, and it does not depend on vanadium surface density. Pure V_2O_5 also exhibits an intrinsic selectivity to C_3H_6 of about 80%, but the corresponding value for ZrV_2O_7 is zero. The data in Fig. 10 show that the rate of propane conversion at each calcination temperature is nearly constant for VO_x surface densities between 1 and 3 V/nm^2, but then decreases at higher surface densities. At a given VO_x surface density, the rate of propane consumption per V atom increases with increasing calcination temperature.

DISCUSSION

The presence of VO_x on ZrO_2 inhibits the transformation of amorphous ZrO_2 to tetragonal ZrO_2 and the transformation of tetragonal to monoclinic ZrO_2. These effects of VO_x are evident from the XRD data shown in Fig. 2. For calcination temperatures of 673 and 773 K, VO_x also inhibits ZrO_2

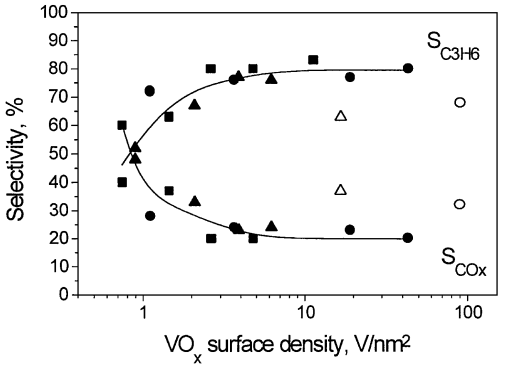

FIG. 9. Propene and CO_x selectivities as functions of VO_x surface density for VO_x/ZrO_2 pretreated at 673 (■), 773 (▲), and 873 K (●). The open symbols represent samples containing a significant amount of ZrV_2O_7.

sintering. However, at high VO_x loadings and particularly after calcination at 873 K, the presence of VO_x causes a loss in surface area, possibly via the progressive formation of ZrV_2O_7.

The structure of VO_x dispersed on ZrO_2 depends on both the surface density of VO_x and the calcination temperature. For surface densities below 2.5 VO_x/nm^2, there is insufficient amount of vanadia on the zirconia surface to form a monolayer. Calcination at 673 K produces an overlayer exhibiting a UV-Vis absorption edge at higher energies that is characteristic of isolated vanadia units (Fig. 6). Consistent with this interpretation, there is no evidence for a band at 860 cm^{-1} in the Raman spectra associated with V–O–V vibrations (see Fig. 4). Calcination of VO_x/ZrO_2 samples containing less than 2.5 VO_x/nm^2 at 773 and 873 K decreases the UV-Vis absorption edge energy and leads to the appearance of a band at 860 cm^{-1} in the Raman spectrum. Both changes are indicative of the formation of small polyvanadate domains. Raising the VO_x surface density from 2.5 VO_x/nm^2 to 7 VO_x/nm^2 ensures the presence of a sufficient number of VO_x units to fully cover the support surface. Consistent with this, the adsorption edge energy

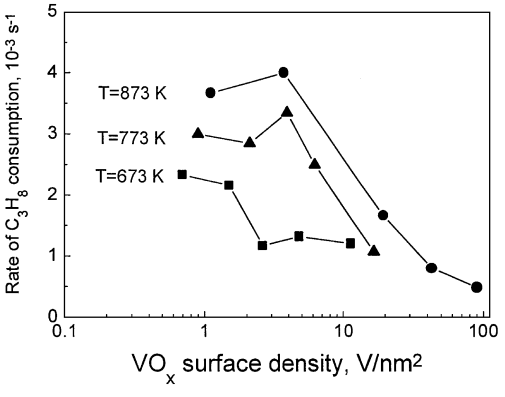

FIG. 10. Dependence of propane conversion rate on VO_x surface density and catalyst calcination temperature.

in the UV-Vis spectrum decreases for a given calcination temperature and a well-defined Raman band is observed at 860 cm^{-1}. For VO_x surface densities greater than 7 VO_x/nm^2, there is no additional decrease in the position of the UV-Vis absorption edge energy and Raman bands now appear for V_2O_5 and ZrV_2O_7. The latter compound is evidenced by peaks at 17.30, 22.36, and 24.63° in the XRD pattern and a band at 780 cm^{-1} in the Raman spectrum. While bulk V_2O_5 was not detected by Raman spectroscopy below an apparent surface density of >7 VO_x/nm^2, this does not preclude the presence of very small particles of V_2O_5 at lower surface densities. As noted in Fig. 9, the propene selectivity on VO_x/ZrO_2 depends only on the VO_x surface density and not on the calcination temperature. At a surface density of 1 VO_x/nm^2, the propene selectivity is 35%, but it increases to a constant value of 80% for surface densities above 2–3 VO_x/nm^2. This latter surface density is within the range expected for monovanadate monolayer coverage of the support. While Fig. 6 shows that the UV-Vis absorption edge energy continues to decrease with increasing calcination temperature and surface density, this seems to have no effect on the propene selectivity. For VO_x surface densities above 10 VO_x/nm^2, the amount of VO_x exceeds that required for a monolayer, but the propene selectivity remains at 80%. The behavior of the propene selectivity with VO_x coverage seen in Fig. 9 suggests that high selectivity may require complete coverage of the ZrO_2 surface by a mixture of vanadate oligomers. It is noted, though, that when the VO_x surface density exceeds 10 VO_x/nm^2, calcination at temperatures above 773 K can lead to the formation of ZrV_2O_7. This compound exhibits a zero selectivity to propene; therefore its formation can lead to a decrease in propene selectivity. This may explain why the two data points shown by open symbols in Fig. 9 lie below the curve describing the rest of the data.

Selectivity and activity data on VO_x/ZrO_2 catalysts can be treated in a more rigorous manner. The oxidative dehydrogenation of propane on VO_x/ZrO_2 catalysts appears to occur via a combination of parallel and sequential oxidation reactions (1, 3, 4):

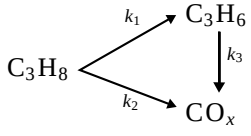

At low propane and oxygen conversions, the concentrations of propane and oxygen are essentially independent of residence time. Thus, assuming first-order kinetics for propane ODH and for combustion of propane and propene, the rates of these reactions can be expressed as follows

$$r_1 = k_1[C_3H_8][O_2]^n = k_1'[C_3H_8] \quad [1]$$

$$r_2 = k_2[C_3H_8][O_2]^m = k_2'[C_3H_8] \quad [2]$$

$$r_3 = k_3[C_3H_6][O_2]^l = k_3'[C_3H_6], \quad [3]$$

where r_I is the rate of reaction i per V atom, [X] is the molar concentration of X and k_i is the pseudo-first order rate coefficient for reaction i.

The rate of propane consumption in a volume element dV of the reactor is given by

$$\frac{Q}{C_V}\frac{d[C_3H_8]}{dV} = r_1 + r_2 = (k_1' + k_2')[C_3H_8], \quad [4]$$

where Q is the volumetric flow rate of gas and C_V is the concentration of V atoms per unit volume of reactor. In a similar manner the rate of propene formation is given by

$$\frac{Q}{C_V}\frac{d[C_3H_6]}{dV} = r_1 - r_3 = k_1'[C_3H_8] - k_3'[C_3H_6], \quad [5]$$

where Q is the gas flow rate and C_V is concentration of V atoms per unit volume of the reactor. Taking $[C_3H_8] = [C_3H_8]_0$ and $[C_3H_6] = 0$ for $V = 0$ and solving Eqs. [4] and [5], one obtains

$$[C_3H_8] = [C_3H_8]_0 \exp(-(k_1' + k_2')C_v\tau) \quad [6]$$

$$[C_3H_6] = [C_3H_8]_0 \frac{k_1'}{k_3' - (k_1' + k_2')} \times (\exp(-(k_1' + k_2')C_V\tau) - \exp(-k_3'C_V\tau)), \quad [7]$$

where $\tau = V/Q$ is the space time.

The propene selectivity is now defined as

$$S_{C_3H_6} = \frac{[C_3H_6]}{[C_3H_8]_0 - [C_3H_8]}. \quad [8]$$

Since the experiments reported here were carried for small conversions of C_3H_8, $S_{C_3H_6}$ is given to good approximation by

$$S_{C_3H_6} = \frac{[C_3H_6]}{(k_1' + k_2')[C_3H_8]_0 C_V\tau}. \quad [9]$$

Substitution of Eq. [7] into Eq. [9] and allowing all exponential terms to be linear for small values of τ gives

$$S_{C_3H_6} = S^0_{C_3H_6}\left(1 - \frac{(k_1' + k_2' + k_3')C_V\tau}{2}\right), \quad [10]$$

where $S^0_{C_3H_6} = k_1'/(k_1' + k_2')$ is the propene selectivity as τ goes to zero.

If $k_3' \gg (k_1' + k_2')$, as will be shown below, then

$$S_{C_3H_6} = S^0_{C_3H_6}\left(1 - \frac{k_3'C_V}{2}\tau\right). \quad [11]$$

The ratio of k_1'/k_2' can then be determined from $S_{C_3H_6}$ measured at zero oxygen conversion, and the value of k_3' from a

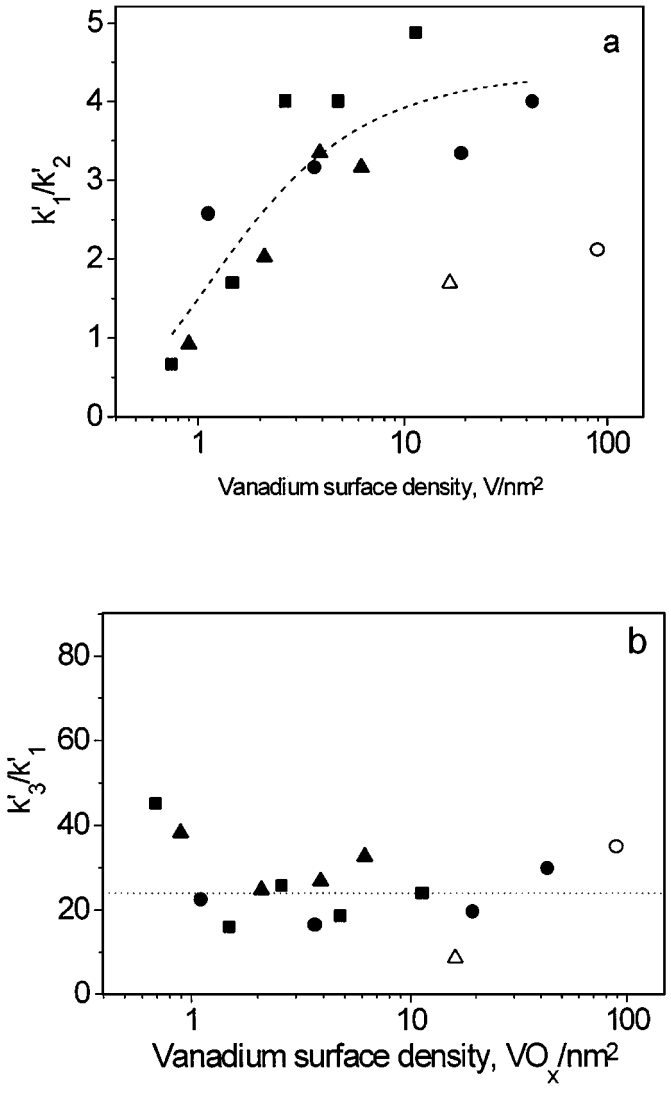

FIG. 11. Dependence of (a) k'_1/k'_2 and (b) k'_3/k'_1 ratios on VO_x surface density for VO_x/ZrO_2 samples pretreated at 673 (■), 773 (▲), and 873 K (●). The open symbols represent samples containing a significant amount of ZrV_2O_7.

plot of $S_{C_3H_6}$ versus reciprocal gas flow rate ($Q^{-1} = \tau / V$). The value of k'_1 can be determined from the rate of propene formation at zero oxygen conversion ($\tau \to 0$). Figure 11 shows plots of k'_1/k'_2 and k'_3/k'_1 as functions of VO_x surface density. The dependence of k'_1/k'_2 on VO_x surface density is very similar to the dependence of propene selectivity seen in Fig. 9 and shows a maximum value of approximately 4 for vanadium surface density, higher than 2–3 VO_x/nm^2. In contrast the value of k'_3/k'_1 is nearly constant at 22, independent of the VO_x surface density. The constancy of k'_3/k'_1 suggests that some sites responsible for propane ODH are involved in the combustion of propene.

The effects of VO_x surface density and calcination temperature on the overall rate of propane conversion per V atom (Fig. 10) can be also attributed to the structure of the VO_x overlayer. For coverages below about 2 VO_x/nm^2, the specific activity is nearly constant, but then decreases monotonically when the VO_x surface density is increased above this level. It is also evident that at a given VO_x surface density, the specific activity increases with increasing calcination temperature. These trends can be explained in the following manner. Up to 2–3 VO_x/nm^2 all of the V atoms are present at the surface of the ZrO_2 either as isolated vanadyl groups or as polyvanadate species. As discussed earlier, the proportion of polyvanadate species increases with increasing calcination temperature for a given VO_x surface density, as evidenced by the decrease in the UV-Vis absorption edge energy. The observed increase in the rate of C_3H_8 conversion rate per V with calcination temperature suggests, therefore, that the oxygen in polyvanadate species is more active than that in isolated vanadyl species. The decrease in specific activity seen above 3–4 VO_x/nm^2 in Fig. 10 is attributed to the formation of multilayers of vanadia, in which not all of the V atoms are exposed to the reactants. Based on these considerations, it is evident that high activity and propene selectivity require V−O−V species in large polyvanadate domains residing on the surface of the ZrO_2 support.

CONCLUSIONS

The structure of vanadia dispersed on zirconia is strongly dependent on the surface density of vanadia and the temperature at which the deposited vanadia has been calcined. Small vanadia clusters, possibly monomeric VO_x species are found in the samples with vanadia loadings lower than that corresponding to a polyvanadate monolayer. Both higher calcination temperatures and higher vanadium contents lead to polyvanadate monolayers. Higher calcination temperatures (873 K) also lead to chemical interaction between VO_x species and zirconia and to a formation of zirconium vanadate. Very low concentrations of bulk V_2O_5 phase are found in the catalysts with high VO_x surface density calcined at higher temperatures (873 K).

Analysis of catalytic and spectroscopic data suggests that polyvanadates species highly dispersed on zirconia are active sites in propane oxidative dehydrogenation. The highest specific activity is observed for a surface density of 3–4 VO_x/nm^2 for VO_x/ZrO_2 calcined at 873 K. The propene selectivity on this catalyst is 80%. At higher VO_x surface densities the specific activity declines monotonically, but the propene selectivity remains constant.

ACKNOWLEDGMENT

This work was supported by the Director, Office of Basic Energy Sciences, Chemical Sciences Division of the U.S. Department of Energy under Contract DE-AC03-76SF00098.

REFERENCES

1. Blasko, T., and López Nieto, J. M., *Appl. Catal.* **157**, 117 (1997).
2. Cavani, F., and Trifiro, F., *Appl. Catal.* **133**, 219 (1995).
3. Kung, H. H., *Adv. Catal.* **40**, 1 (1994).
4. Albonetti, S., Cavani, F., and Trifiro, F., *Catal. Rev.-Sci. Eng.* **38**, 413 (1996).
5. Mamedov, E. A., and Cortés-Corberàn, V., *Appl. Catal.* **127**, 1 (1995).
6. Busca, G., *Catal. Today* **27**, 457 (1996).
7. Deo, G., and Wachs, I. E., *J. Phys. Chem.* **95**, 5889 (1991).
8. Corma, A., López Nieto, J. M., Paredes, N., Shen, Y., Cao, H., and Suib, S. L., *Stud. Surf. Sci. Catal.* **72**, 213 (1992).
9. Centi, G., and Trifiro, F., *Appl. Catal. A: General* **143**, 3 (1996).
10. Michalakos, P., Kung, M. C., Jahan, I., and Kung, H. H., *J. Catal.* **140**, 226 (1993).
11. Owens, L., and Kung, H. H., *J. Catal.* **148**, 587 (1994).
12. Corma, A., López Nieto, J. M., and Paredez, N., *J. Catal.* **144**, 425 (1993).
13. Sananes-Schulz, M. T., Tuel, A., Hutchings, G. J., and Volta, J. C., *J. Catal.* **166**, 388 (1997).
14. Zatorski, L. W., Centi, G., López Nieto, J. M., Trifiro, F., Belussi, G., and Fattore, V., *Stud. Surf. Sci. Catal.* **49**, 1243 (1989).
15. Gao, X., Ruiz, P., Xin, Q., Guo, X., and Delmon, B., *J. Catal.* **148**, 56 (1995).
16. Hanuza, J., Jezowska-Trzebiatowska, B., and Oganowski, W., *J. Mol. Catal.* **29**, 109 (1985).
17. Blasko, T., Concepción, P., López Nieto, J. M., and Pérez-Pariente, J., *J. Catal.* **152**, 1 (1995).
18. Centi, G., *Appl. Catal. A: General* **147**, 267 (1996).
19. Wachs, I. E., and Weckhuysen, B. M., *Appl. Catal. A: General* **157**, 67 (1997).
20. Centi, G., Perathoner, S., Trifiro, F., Aboukais, A., Aissi, C. F., and Guelton, M., *J. Phys. Chem.* **96**, 2617 (1992).
21. Sanati, M., Andersson, A., Wallenberg, L. R., and Rebenstorf, B., *Appl. Catal. A: General* **106**, 51 (1993).
22. Sohn, J. R., Gho, S. G., Pae, Y. I., and Hayashi, S., *J. Catal.* **159**, 170 (1996).
23. Schart, U., Schrami-Marth, M., Wokaun, A., and Baiker, A., *J. Chem. Soc. Faraday Trans.* **87**, 3299 (1991).
24. Mercera, P. D. L., van Ommen, J. G., Desburg, E. B. M., Burggraaf, A. J., and Ross, J. R. H., *Appl. Catal.* **57**, 127 (1990).
25. Mercera, P. D. L., van Ommen, J. G., Desburg, E. B. M., Burggraaf, A. J., and Ross, J. R. H., *Appl. Catal.* **71**, 363 (1991).
26. Iglesia, E., Barton, D. G., Soled, S. L., Miseo, S., Baumgartner, J. E., Gates, W. E., Fuentes, G. A., and Meitzner, G. D., *Stud. Surf. Sci. Catal.* **101**, 533 (1996).
27. Meunier, F. C., Yasmeen, A., and Ross, J. R. H., *Catal. Today* **37**, 33 (1997).
28. Ted Oyama, S., Went, G. T., Lewis, K. B., Bell, A. T., and Somorjai, G., *J. Phys. Chem.* **93**, 6786 (1989).
29. Su, S., Carstens, J. N., and Bell, A. T., *J. Catal.*, submitted.
30. Delgass, W. N., "Spectroscopy in Heterogeneous Catalysis," Academic Press, New York, 1979.
31. Toraya, H., Yoshimura, M., and Somiya, S., *J. Amer. Ceram. Soc. C*, 119 (1984).
32. Keramidas, V. G., and White, W. B., *J. Amer. Ceram. Soc.* **57**, 22 (1974).
33. Roozeboom, F., Mittelmeijer-Hazelger, M. C., Moulijn, J. A., de Beer, J., and Gellings, P. J., *J. Phys. Chem.* **84**, 2783 (1980).
34. Went, G. T., Oyama, S. T., and Bell, A. T., *J. Phys. Chem.* **94**, 4240 (1990).
35. Good, M. L., *Spectrochim. Acta A* **29**, 707 (1973).
36. So, H., and Pope, M. T., *Inorg. Chem.* **11**, 1441 (1972).
37. Iwamoto, M., Furukawa, H., Matsukami, K., Takenaka, T., and Kagawa, S., *J. Amer. Chem. Soc.* **105**, 3719 (1983).
38. Ronde, H., and Snijders, J. G., *Chem. Phys. Lett.* **50**, 282 (1977).
39. Cherstnoy, N., Hull, R., and Brus, L. E., *J. Chem. Phys.* **85**, 2237 (1986).
40. Alivasatos, A. P., *Science* **271**, 933 (1996).
41. Service, R. F., *Science* **271**, 920 (1996).
42. Hoener, C. F., Allan, K. A., Bard, A. J., Campion, A., Fox, M. A., Mallouk, T. E., Webber, S. E., and White, J. M., *J. Phys. Chem.* **96**, 3812 (1992).
43. Liu, Z., and Davis, R. J., *J. Phys. Chem.* **90**, 2555 (1986).
44. Wang, Y., Mahler, S. W., and Kasowski, R., *J. Chem. Phys.* **87**, 7315 (1987).
45. Weber, R. S., *J. Catal.* **151**, 470 (1995).
46. Fournier, M., Louis, C., Che, M., Chaquin, P., and Masure, P., *J. Catal.* **119**, 400 (1989).
47. Demuynck, J., Kaufmann, G., and Brunette, J.-P., *Bull. Soc. Chim. France* **11**, 3840 (1969).
48. Bendoraitis, J. G., and Salomon, R. E., *J. Phys. Chem.* **69**, 3666 (1965).